JOURNAL OF MATERIALS SCIENCE 21 (1986) 2697–2704

A comparison between ion implantation and laser alloying of pure iron for oxidation resistance improvement

Part 1 *Boron alloying*

M. PONS, A. GALERIE, M. CAILLET
Laboratoire d'Adsorption et Réaction de Gaz sur Solides, ENS d'Electrochimie et d'Electrométallurgie de Grenoble–INPG, BP 75, 38402 Saint Martin d'Hères, France

We used boron implantation or boron laser alloying to increase the thermal oxidation resistance of iron. Both surface treatments are shown to have a great efficiency. The boron-containing phases formed at the substrate-scale interface are responsible for the observed protection.

1. Introduction

The modification of the surface properties of solids takes an increasing part in the field of materials science. For several years, energetic beams (laser, ions, electrons) have been used for this purpose on a laboratory stage and are now entering pilot or production lines [1–4]. Such beams allow easy modifications of surface composition without any change in the bulk properties of the materials. Catalytic, optical, corrosion or wear performances can thus be adjusted.

We have used ion implantation to increase the thermal oxidation resistance of several metals, and showed that in some cases the efficiency of this treatment was excellent [5–9]. The aim of the work presented here was to determine whether, in some cases, laser alloying could lead to comparable results.

Ion implantation induces a mechanical mixing at the surface of the material, resulting also in the formation of many defects [10, 11]. The nature of the phases produced is governed by the processes of nuclear collision and electronic stopping only. The surface alloy composition can thus be out of equilibrium [12–16].

On the other hand, the laser treatment of a compound deposited on a metal surface leads to the melting of the surface. The melted layer then solidifies quickly. The rate of solidification is the important parameter controlling the alloy composition. If this rate is high enough, new phases out of equilibrium can also be obtained [17, 18]. In this treatment, the transformed thickness (0.1 to 1 mm) is much more important than in the case of ion implantation ($< 1\,\mu m$).

We present here experimental results concerning the alloying of boron into an iron matrix using these two techniques, and compare the effects on the high-temperature oxidation behaviour of iron.

2. Experimental procedure

2.1. Ion implantation

Iron was supplied in the form of foils ($100\,\mu m$ in thickness) with a purity of 99.5%. Implantation was performed [19] at 100 keV with mono-charged boron ions; the beam current was $4\,\mu A\,cm^{-2}$. The maximum dose was $1 \times 10^{17} B^+\,cm^{-2}$, corresponding to $\sim 1.8\,\mu g\,cm^{-2}$. The temperature rise measured by a thermocouple in a region of the sample masked from the beam never exceeded 300° C during the treatment, and the vacuum was kept at $\sim 1 \times 10^{-6}$ mbar (10^{-4} Pa).

2.2. Laser treatment

The c.w. Nd-YAG laser used in this study has been described previously [19]. It operates at a wavelength of $1.06\,\mu m$, with a maximum power of 30 W. The laser beam collimated to an area of $400\,\mu m$ in diameter is fixed and the sample moves in front of it with a speed of $1\,cm\,sec^{-1}$. The duration of the illumination of a particular point on the metal surface is therefore 40 msec. To prevent any deformation of the sample during the treatment, thick foils were used here (1.5 mm). No temperature measurements of the treated surface could be done. The maximum temperature rise of the bulk of the sample was $\sim 80°$ C.

Small grains of boron ($50\,\mu m$ diameter) were added to pure ethanol at a concentration of $10\,g\,l^{-1}$. After ultrasonic mixing, the suspension was deposited onto the iron samples ($\sim 0.2\,cm^3\,cm^{-2}$) and the ethanol evaporated. The boron grains were observed to have a uniform distribution on the metal surface [20] with a coverage ratio of 20 to 30%, in good agreement with the calculated value (25%) (Fig. 1). A comparison of the respective diameters of the beam ($400\,\mu m$) and of the boron particles ($50\,\mu m$) leads to the conclusion that, at a given time of treatment, any boron particle was surrounded by a molten zone of iron.

To prevent thermal oxidation during the treatment, argon was used as a shielding gas.

2.3. Profiling experiments

Profiling of the samples was achieved before and after thermal oxidation by glow-discharge optical spectrometry [19]. This method allows the simultaneous

0022–2461/86 $03.00 + .12

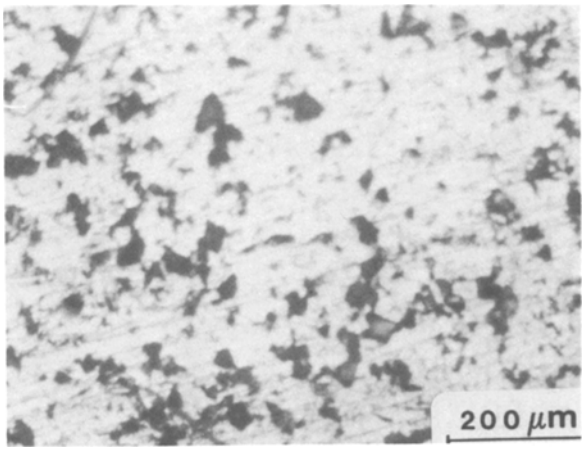

Figure 1 Boron grains on the iron surface before laser treatment (boron appears black on the photograph).

recording of the boron, iron and oxygen profiles by sputtering the target. The possibility of following the oxygen concentration allows the precise determination of the position of the oxide-scale interface of the oxidized samples. Thickness calibrations could be obtained with implanted standard specimens or by microscopically checking the thickness of the oxide scales.

3. The iron–boron and iron–boron–oxygen systems

Two compounds, Fe_2B and FeB, appear in the iron–boron phase diagram [21–23]. When implanted, according to Sood [24], boron must be located mainly in interstitial positions, due to its low atomic radius compared with that of iron. This fact was experimentally confirmed by the work of Andersen *et al.* [25].

As boron has a very low solubility in iron, structural transformations are expected during boron implantation or alloying by laser treatment. Stable borides may appear, but phases out of equilibrium or even amorphous material [26, 27] may be observed.

Five iron borates have been described in the literature [28]: Fe_3BO_5, Fe_3BO_6, $FeBO_3$, FeB_2O_4 and FeB_4O_7.

Unfortunately, the thermodynamic functions of these compounds are not known and it was impossible to draw any stability diagram. However, experimental work under hydrothermal conditions [29] has shown that FeB_4O_7 and Fe_3BO_5 are stable between 450 and 700° C. It may be recalled here that Rolls and Shaw [30, 31] observed Fe_3BO_5 as the oxidation product of a boron containing coating on iron.

A possible diagram for the system Fe_2O_3–B_2O_3 was proposed by Joubert *et al.* [32]. In this diagram $FeBO_3$ is shown to decompose at 930° C to give Fe_3BO_6.

4. Study of the iron samples after treatment

4.1. After boron implantation

The profile of the boron atoms after implantation (concentration against depth) is given by

$$C(x) = \frac{\Phi}{(2\pi)^{1/2}\Delta R_p \varrho} \exp\left(-\frac{(x - R_p)^2}{2\Delta R_p^2}\right)$$

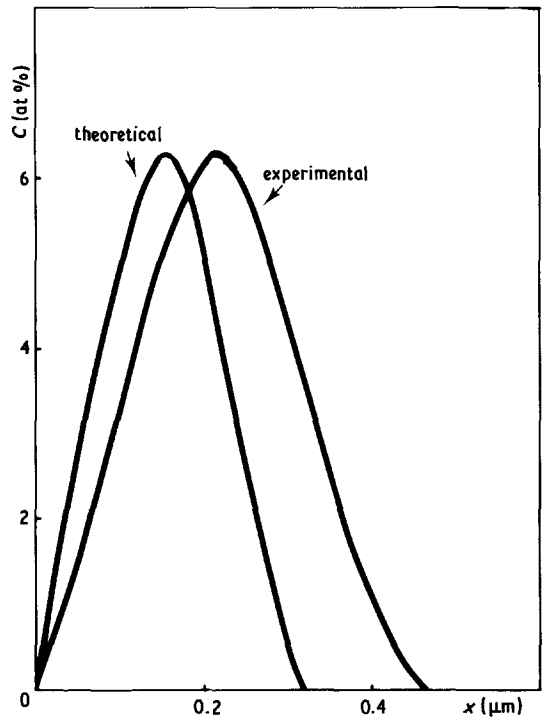

Figure 2 Boron profile after ion implantation.

where Φ is the implantation dose (at cm^{-2}), ϱ the atomic density of the iron matrix (at cm^{-3}), R_p the mean projected range of the ions and ΔR_p the standard deviation. These last values have been calculated by the Manning and Mueller procedure [33] to give $R_p = 0.1525\,\mu m$, $\Delta R_p = 0.0845\,\mu m$ for an implantation energy of 100 keV. The derived theoretical boron profile for a dose of 1×10^{17} B$^+$ cm^{-2} is shown in Fig. 2.

The actual profile for the same dose observed by glow-discharge optical spectrometry is also approximately gaussian (Fig. 2) with measured values of $R_p \sim 0.22\,\mu m$ and $\Delta R_p \sim 0.1\,\mu m$. The precision of this measurement is not very good ($\sim 20\%$) but it is clear that the experimental values are greater than the theoretical ones, contrary to what is generally observed for sputtering of a surface by an ion beam. This fact is not surprising, due to the very approximate values of the stopping coefficients used in the calculations. It is well known that these coefficients are not very accurate for light ions.

The phases which are formed during boron implantation into iron have been characterized by Ali *et al.* [34] and Kolitsh *et al.* [26]. The results of this last work are presented in Fig. 3, and show that, under our implantation conditions (1×10^{17} B$^+$ cm^{-2}), the formation of amorphous FeB is expected. The amorphicity may be explained by the thermal spike occurring in the elementary cascades and the high resulting cooling rates ($\sim 10^{11}$ K sec^{-1}) [1].

In good agreement with this diagram, glancing-angle X-ray diffraction experiments always failed to identify crystallized borides, even when implantation was formed to a dose of 1×10^{17} B$^+$ cm^{-2}.

4.2. After laser alloying

The observation of cross-sections of samples boronized by laser alloying with a power density of 2.5 ×

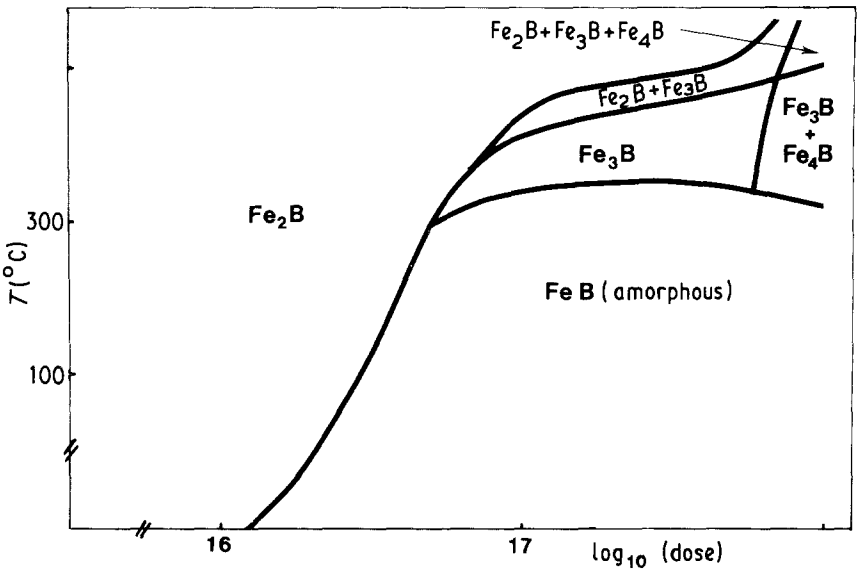

Figure 3 Stability diagram for the Fe–B system achieved by ion implantation (from Kolitsh *et al.* [26]).

$10^8\,W\,m^{-2}$, and a translation speed of $1\,cm\,sec^{-1}$, shows three different zones (Figs 4b and c):

(a) a near-surface region, containing all boron, with a thickness of 20 μm (Region 3);

(b) a coarse-grained intermediate region, melted during the treatment but where no Fe–B mixing occurred (Region 2); and

(c) the iron substrate not affected by the treatment (Region 1).

X-ray diffraction analysis showed the presence of

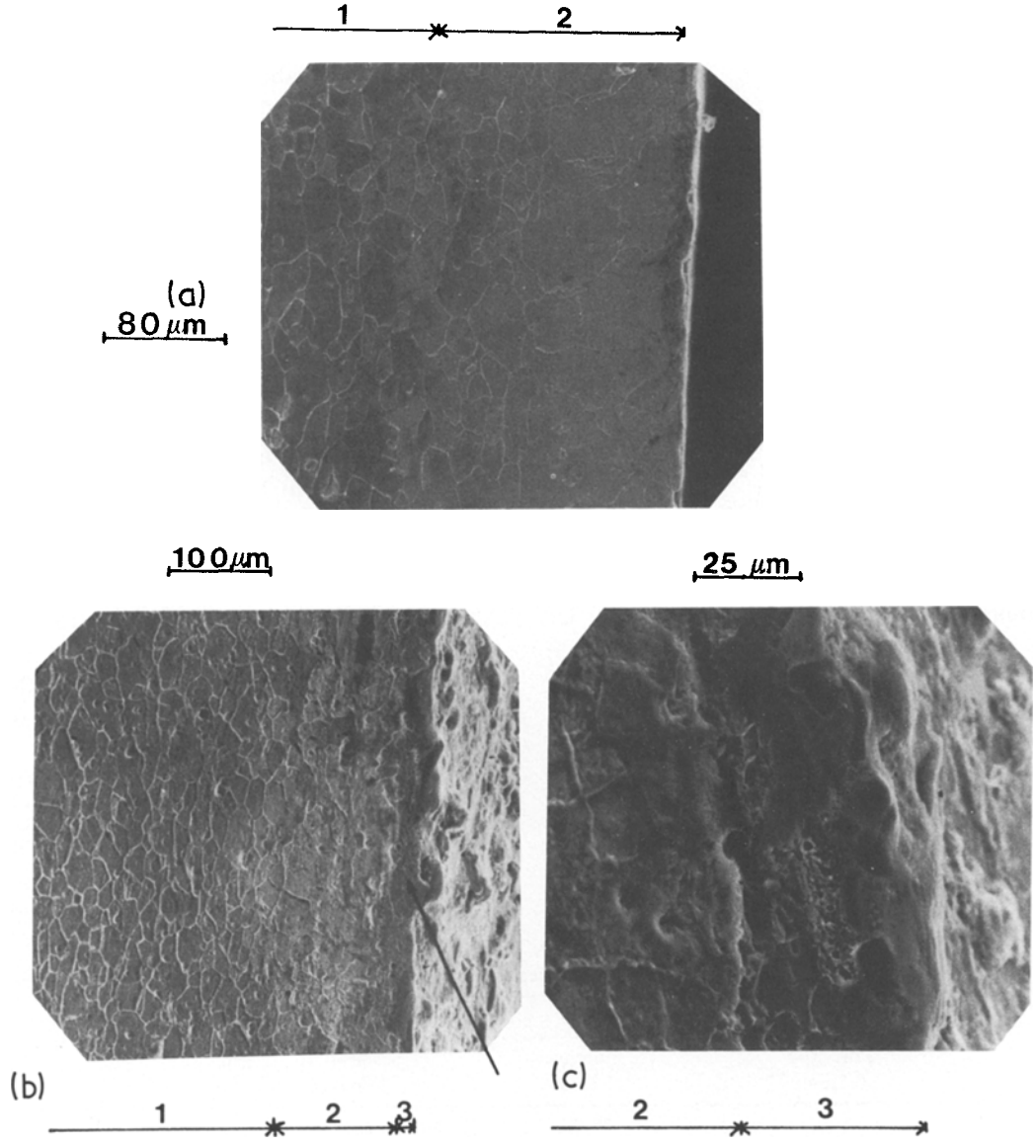

Figure 4 Microscopic examination (SEM) of cross-sections of (a) iron and (b, c) boronized iron (nital etched). Region 1 = non-melted zone, Region 2 = melted zone, Region 3 = boronized zone. The arrow in (b) shows the region enlarged in (c).

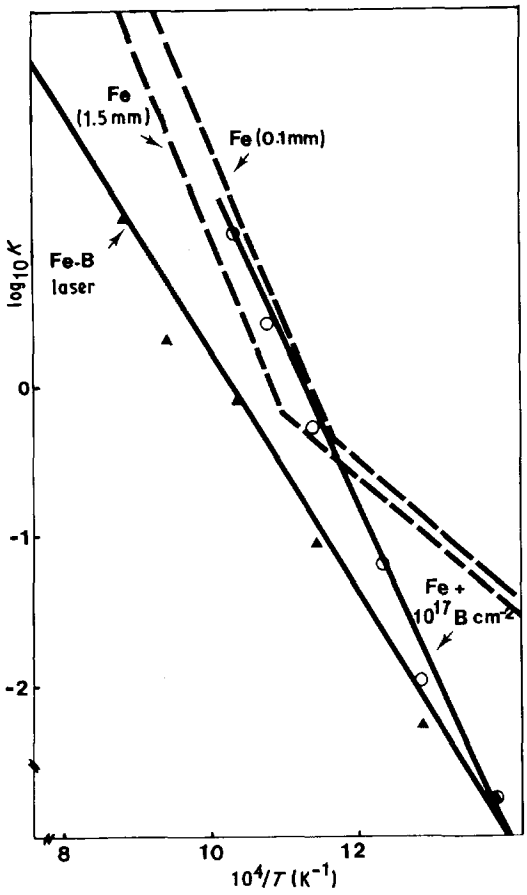

Figure 5 Oxidation of implanted and laser-treated iron: Arrhenius plot for the parabolic rate constant K (mg^2 cm^{-4} h^{-1}) (oxidation time ~ 5 h). Precision on log K: ± 0.2. Error bars have been omitted for better clarity.

Fe_2B and FeB in the boron-containing layer. Elementary boron no longer appeared and had therefore entirely reacted with iron in the molten layer. Traces of B_2O_3 were always observed, resulting from the presence of some remaining oxygen in the shielding gas.

The cooling rate could be evaluated as 10^5 K sec^{-1} under our experimental conditions, and was too low to induce the formation of amorphous phases.

The results of the two treatments can therefore be summarized as follows:

1. Ion implantation (100 keV, 4 μA cm^{-2}, 300° C, 1×10^{17} B$^+$ cm^{-2}) leads to the formation of an amorphous phase, where the boron concentration is a maximum (6.3 at %) at a depth of ~ 200 nm, and falls to zero at a depth of 400 nm.

2. Laser alloying (power density 2.5×10^8 W m^{-2}, interaction time 0.04 sec) leads to the formation of a mixture of FeB and Fe_2B to a depth of 20 μm. In this region the boron concentration is ~ 40%, much higher than in the implanted samples.

The results of both treatments are therefore very different.

5. Thermal oxidation kinetics

Boron implantation has been shown to improve considerably the oxidation behaviour of pure iron, as soon as the dose reaches 10^{15} B$^+$ cm^{-2} [9]. The observed protection increases with the dose and remains even when the corroded layer is several times thicker than the implanted zone. At a dose of 1×10^{17} B$^+$ cm^{-2} the protection afforded is excellent, as the weight gain observed on pure iron after two hours at 540° C is only achieved with implanted samples after 100 h at the same temperature. This protection was observed in the 400 to 700° C temperature range.

Boron alloying has also been observed to improve the corrosion resistance of iron in the 500 to 900° C temperature range [20]. At 600° C the protection is of the same order as that observed on implanted samples. It is better at higher temperatures.

5.1. Initiation of the oxidation

For technical reasons, the iron foils used for implantation experiments had to be thin (the area of lateral faces could be neglected), whereas those used for laser treatments had to be thicker. Both kinds of iron oxidized parabolically, but some discrepancies were observed in the parabolic rate constants. However, the measured activation energies were always the same.

As the samples boronized by the two techniques oxidized parabolically during a few hours (20 h at 500° C, 5 h at 850° C), an Arrhenius diagram can represent the comparative results of the two treatments (Fig. 5). It can be seen that the rate constant for pure iron oxidation exhibits two different activation energies, whereas the constant for the oxidation of the samples boronized by both techniques exhibits one activation energy only. Table I summarizes the results.

Boron implantation lowers the parabolic rate constant at temperatures under 600° C only, whereas laser alloying lowers it at any temperature in the 300 to 800° C range.

5.2. Extended times of oxidation

After the initial parabolic period, the rate of reaction of the boronized samples diminishes more than required by a parabolic law. At this time the increase in the weight gain becomes very low and the protection afforded is therefore good. This can be seen in Fig. 6, where the gravimetric curves concerning pure iron, iron implanted with 1×10^{17} B$^+$ cm^{-2} or laser-alloyed iron are presented in parabolic coordinates. The observed blocking effect is effective over the whole temperature range explored (Figs 7 and 8).

TABLE I Oxidation of pure or boronized iron. Activation energies from the parabolic rate constants

Temperature (° C)	Activation energy (kJ mol^{-1})			
	Pure iron (0.1 mm)	Pure iron (1.5 mm)	Fe + 10^{17} B$^+$ cm^{-2} (implanted)	Fe–B (laser-alloyed)
400 to ~ 600	85	75	221	159
~ 600 to 800	225	230	221	159
Above 800	–	230	–	159

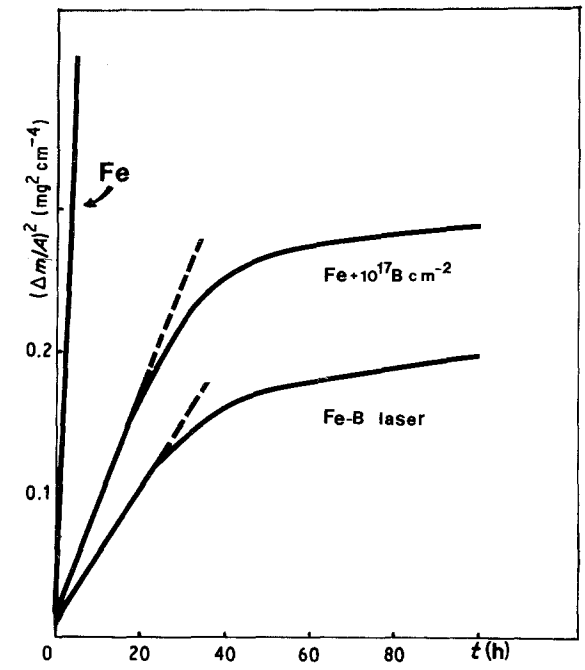

Figure 6 Oxidation of implanted and laser-treated iron: parabolic plots (T = 500° C, P_{O_2} = 100 torr).

The efficiency of the treatment can be defined as the difference between the oxygen mass fixed on pure iron and on the boronized samples under the same conditions. This efficiency, normalized to the weight gain of pure iron, is shown in Figs 9 and 10 and is seen to be a maximum at low temperatures for both treatments.

5.3. Overall rate law

Two successive periods have been shown to occur during the oxidation of iron boronized either by implantation or by laser alloying: a parabolic period, followed by a quickly decreasing rate leading to a blocking of the reaction. The equation

$$\Delta m/A = k_1[1 - \exp(-k_2 t)] \quad (1)$$

TABLE II Values of k_1 and k_2 obtained by minimization of F (Equation 2) for the two systems

Material	T (° C)	k_1 (mg cm^{-2})	k_2 (h^{-1})
Fe–B (laser-alloyed)	500	0.39	0.078
	540	0.95	0.167
	600	1.47	0.096
	700	3.06	0.162
	815	14.40	0.049
	860	19.35	0.362
Fe + 10^{17} B$^+$ cm^{-2}	500	1.072	0.0127
	570	1.325	0.1308
	650	4.645	0.2500
	690	6.997	0.2477

where $\Delta m/A$ is the mass change per unit area, t is time and k_1, k_2 are constants can fit the overall experimental gravimetric curves. Such a formulation does not correspond to the actual physical phenomena but has the advantage of describing all the rate law by a unique formula.

The constants k_1 and k_2 were determined by a computer calculation [35], minimizing the expression

$$F = \sum_{t_{min}}^{t_{max}} [(\Delta m/A)_{exp} - (\Delta m/A)_{theoret}]^2 \quad (2)$$

The values of k_1 and k_2 obtained for different temperatures are reported in Table II.

6. Nature and distribution of the products formed during oxidation of the boronized samples

6.1. Oxidation of implanted iron

Glancing-angle X-ray diffraction experiments (~ 10°) showed that the nature of the phases formed during oxidation depended on its duration.

For low times of oxidation (1 h at 540° C, for example), besides the iron oxides, the iron borate FeB_4O_7 could be identified. This compound is the most boron-containing of the five known borates.

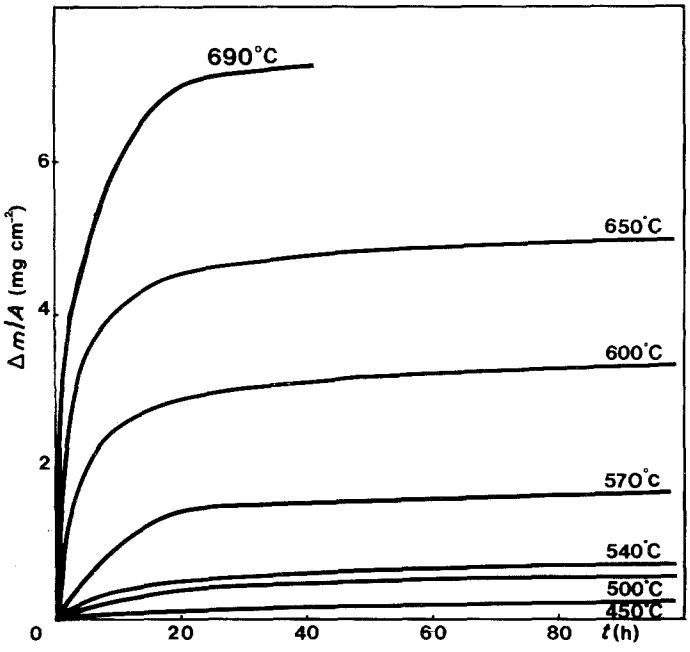

Figure 7 Oxidation of boron-implanted iron (Fe + 10^{17} B$^+$ cm^{-2}, P_{O_2} = 100 torr): influence of the temperature.

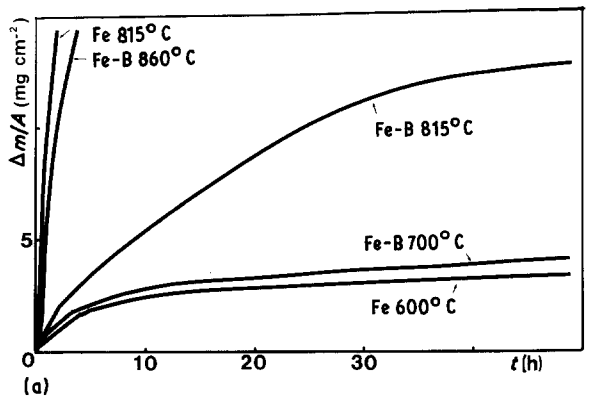

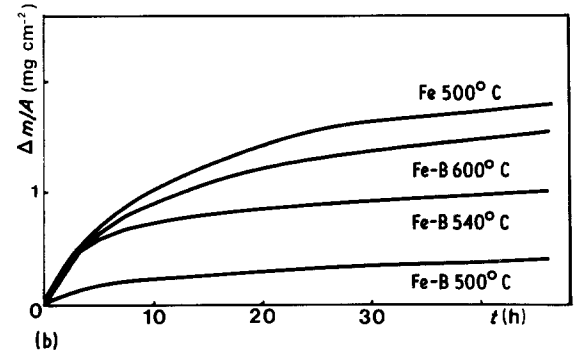

Figure 8 (a, b) Oxidation of laser-boronized iron (P_{O_2} = 100 torr): influence of the temperature.

As the oxidation proceeded, this borate transformed slowly into FeB_2O_4. At the end of the parabolic period, FeB_2O_4 only was observed. This compound was therefore responsible for the observed blocking effect. By glow-discharge optical spectrometry profiling, it was observed that this compound was located at the metal–oxide interface of the corrosion scale (Fig. 11).

6.2. Oxidation of laser-alloyed iron

In this case also, the nature of the formed products was dependent on the duration of the reaction.

For low oxidation times (< 1 h at 500° C), iron oxides were naturally observed, mixed with B_2O_3, but B_6O was also present in contact with the boronized substrate.

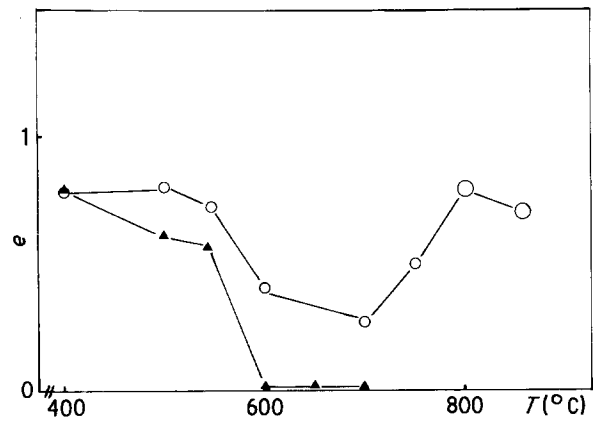

Figure 9 Normalized efficiency $e = [(\Delta m/A)_{Fe} - (\Delta m/A)_{Fe-B}]/(\Delta m/A)_{Fe}$ of the treatments for an oxidation time of 5 h. Precision on e values: ±0.1. Error bars have been omitted for better clarity. (○) Laser. (▲) implantation.

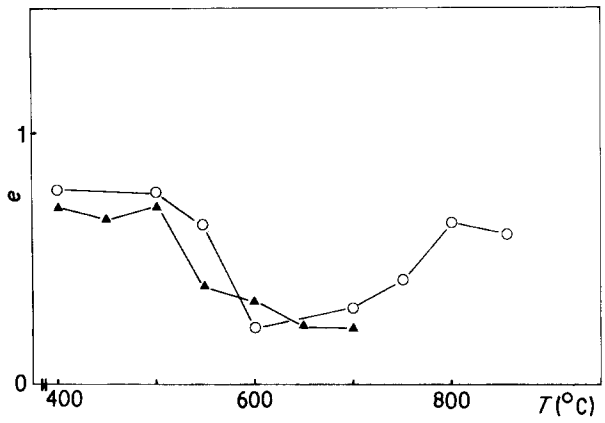

Figure 10 Normalized efficiency (e) (see Fig. 9) of the treatments for an oxidation time of 50 h. Precision on e values: ±0.1. Error bars have been omitted for better clarity. (○) Laser, (▲) implantation.

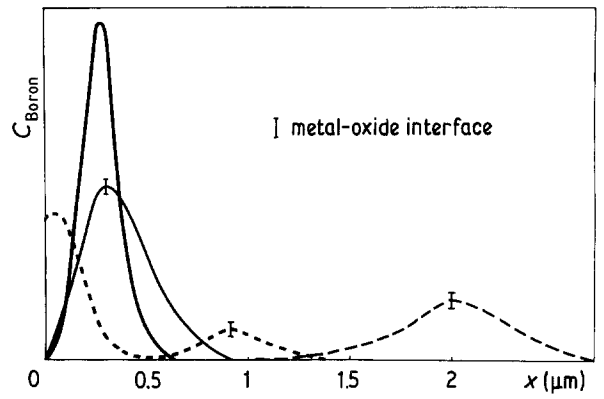

Figure 11 Boron profiles after oxidation of iron implanted with 1×10^{17} at cm^{-2} at 600° C and P_{O_2} = 100 torr. t = (—) 0, (—) 5 min, (- - - -) 20 min, (––) 1 h.

When the oxidation proceeded for longer times, B_6O and B_2O_3 disappeared, and $FeBO_3$ and Fe_3BO_5 appeared.

It must be observed that FeO was never observed on the boronized samples, even at temperatures where it was stable, contrary to what was observed on pure iron (Figs 12 and 13).

The location of the borates in the corrosion scale was found to be (i) for Fe_3BO_5: near the metal substrate, and (ii) for $FeBO_3$: mixed with Fe_3O_4 and Fe_2O_3 within the overall oxide scale.

The nature and location of the products formed is compared for both treatments in Table III.

It is easy to see from this table that two major differences exist concerning (a) the nature of the formed products (FeB_2O_4 for ion-implanted iron or Fe_3BO_5 and $FeBO_3$ for laser-alloyed iron), and (b) the location of the borates (near the internal interface only for ion-implanted iron, in the overall oxidation layer for laser-alloyed iron).

TABLE III Nature and location of the products formed at the end of the oxidation experiments

Implantation	Laser alloying	Location
FeB_2O_4	Fe_3BO_5	Metal–scale interface
FeO ($T \geqslant 600°$ C)	Fe_3O_4, Fe_2O_3	Heart of the scale
Fe_3O_4	$FeBO_3$	Heart of the scale
Fe_2O_3	B_2O_3 ($T \leqslant 650°$ C)	Heart of the scale

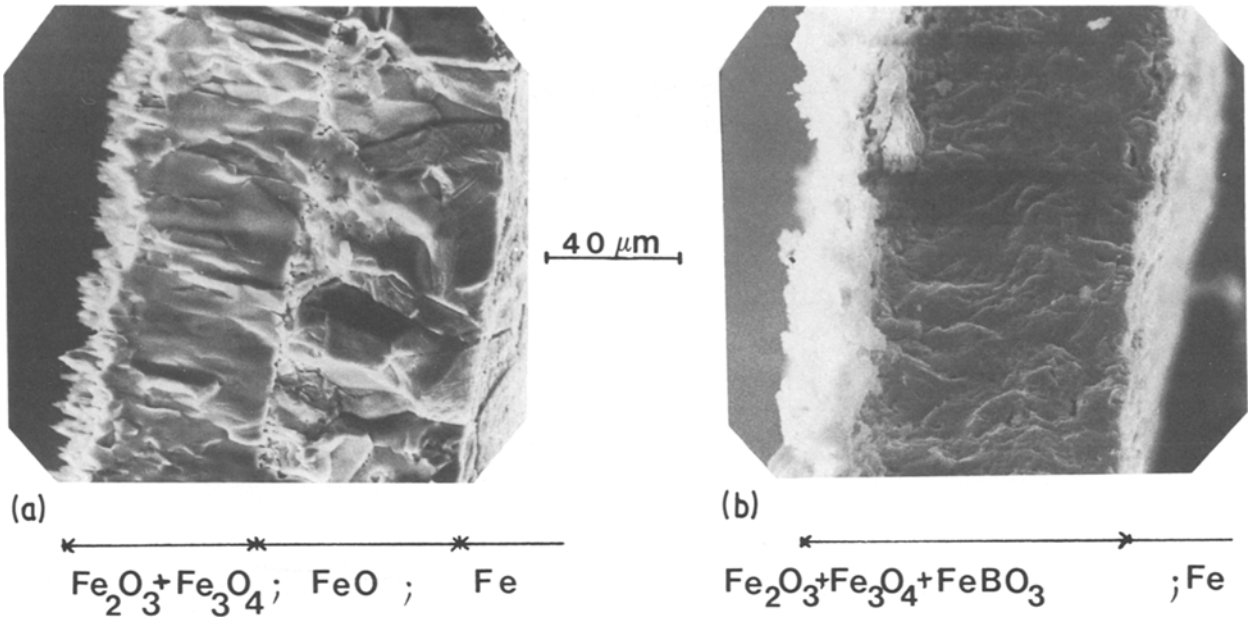

Figure 12 Microscopic examination (SEM) of oxide layers on (a) pure iron and (b) laser-treated iron, showing the absence of FeO in the scale growing on boronized iron. T = 815° C, oxidation time 50 h.

7. Discussion

Both surface treatments studied here have been shown to have a great efficiency in preventing the thermal oxidation of iron. However, the similar rate-laws observed are the results of the growing of very different oxide scales. It is well known that the oxidation of iron proceeds by outward cation diffusion, and evidence arises from the results that the borates that are formed inhibit this diffusion. The comparison between the efficiency of the two treatments shows that the phase formed at the substrate–scale interface (FeB_2O_4 or Fe_3BO_5) is responsible for this protection.

In the case of the boron-implanted specimens, due to the very low amount of boron involved, FeB_2O_4 is entirely trapped in the voids formed in the substrate by an internal interfacial reaction (jumping of iron atoms from the metal to the corrosion scale). The very low B/Fe ratio allows the formation of all stable iron oxides. FeO is therefore normally observed above its decomposition temperature.

For the laser-boronized samples, $FeBO_3$ is observed throughout the corrosion scale, as a result of the high amount of boron introduced by the treatment. The reduction of this compound by FeO is possible in the internal part of the scale according to the reaction $FeBO_3 + 2FeO \rightarrow Fe_3BO_5$.

This mechanism probably accounts for the absence of FeO in the scale.

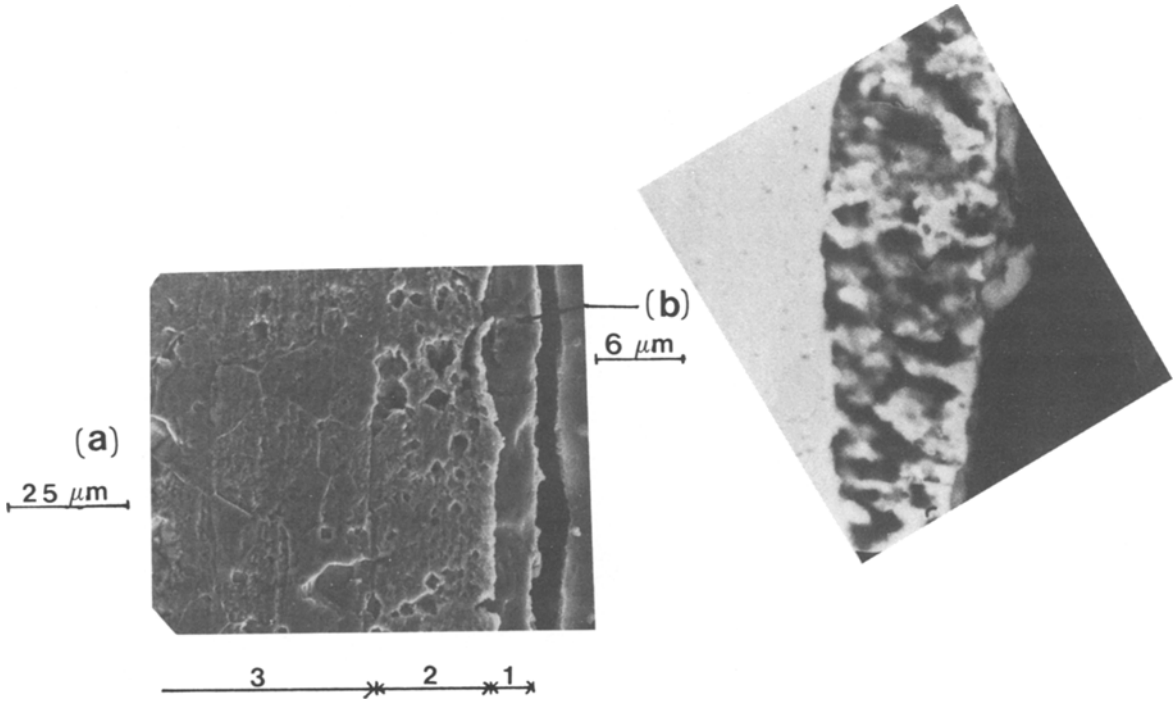

Figure 13 (a) Microscopic examination (SEM) and (b) backscattered electron image of an oxide layer grown on laser-boronized iron. Region 1 = oxide, Region 2 = melted zone, Region 3 = non-melted zone. T = 600° C, oxidation time 50 h.

Acknowledgements

The authors thank Mr Goussis for numerical calculations, and Drs Bruel and Gailliard (CEN–Grenoble) for kindly performing the implantation.

References

1. S. T. PICRAUX, *Ann. Rev. Mater. Sci.* **14** (1984) 355.
2. B. BIASSE, G. DESTEFANIS and J. P. GAILLIARD (editors), "Ion Beam Modification of Materials", Grenoble, 1982 (North-Holland, Amsterdam, 1983).
3. K. MUKHERJEE and J. MAZUMDER (editors), "Lasers in Metallurgy", Chicago, 1981 (Metallurgical Society of AIME, 1981).
4. S. T. PICRAUX, in "Distinguished Lecture Series in Industrial Materials Science and Engineering", edited by L. E. Murr (Dekker, New York, 1984).
5. M. PONS, A. GALERIE and M. CAILLET, *Corrosion Sci.* **22**(3) (1982) 239.
6. *Idem, Nucl. Inst. Meth.* **209/210** (1983) 1011.
7. *Idem, Corrosion Sci.* **23**(11) (1983) 1181.
8. *Idem, Ann. Chim. Fr.* **9** (1984) 567.
9. *Idem, ibid.* **7** (1982) 15.
10. A. D. MARWICK, *Nucl. Inst. Meth.* **182/183** (1981) 827.
11. S. MATTESON and M. A. NICOLET, *Ann. Rev. Mater. Sci.* **13** (1983) 339.
12. S. M. MYERS, *J. Vac. Sci. Technol.* **17**(1) (1980) 310.
13. *Idem, Nucl. Inst. Meth.* **168** (1980) 265.
14. E. N. KAUFMAN and L. BUENE, *ibid.* **182/183** (1981) 327.
15. W. A. GRANT, *ibid.* **182/183** (1981) 809.
16. J. A. BORDERS, *Ann. Rev. Mater. Sci.* **9** (1981) 313.
17. S. D. FERRIS, H. J. LEAMY and J. M. POATE (eds), "Laser–Solid Interactions and Laser Processing", Boston, 1978, AIP Conference Proceedings No. 50 (American Institute of Physics, New York, 1979).
18. B. H. KEAR, B. C. GIESSEN and M. COHEN (editors), "Rapidly Solidified Amorphous and Crystalline Alloys", Boston, 1981 (Elsevier, 1982).
19. M. PONS, thèse Docteur-Ingénieur, University of Grenoble (1982).
20. M. PONS, A. GALERIE and M. CAILLET, *Mater. Techn.* **12** (1985) 699.
21. M. HANSEN, "Constitution of Binary Alloys" (McGraw-Hill, New York, 1958) p. 249.
22. R. P. ELLIOT, "Constitution of Binary Alloys", 1st Supplement (McGraw-Hill, New York, 1965) p. 119.
23. F. A. SHUNK, "Constitution of Binary Alloys", 2nd Supplement (McGraw-Hill, New York, 1969) p. 86.
24. D. K. SOOD, *Proc. Nucl. Phys. Sol. State Phys. Symp.* **20C** (1977) 376.
25. J. V. ANDERSEN, E. LOOGSGAARD and L. C. FELDMAN, *Rad. Eff.* **12** (1972) 219.
26. A. KOLITSH, B. RAUCHENBACH and E. RITCHER, *Rad. Eff. Lett.* **16**(6) (1983) 193.
27. V. KOSTER, V. HEROLD and D. KRANSE, in "Rapidly Solidified Amorphous and Crystalline Alloys", Boston, 1981, edited by B. H. Kear, B. C. Giessen and M. Cohen (Elsevier, 1982) p. 179.
28. Power diffraction file, Cards 25-395, 18-636, 21-423, 3-186, 21-422 (JCPDS, 1601 Park Lane, Swarthmore, Pennsylvania).
29. T. A. KRAVCHUK and Y. V. D. LAZEBNICK, *Russ. J. Inorg. Chem.* **12**(1) (1967) 21.
30. R. ROLLS and R. D. SHAW, *Nature* **229** (1971) 192.
31. *Idem, Corrosion Sci.* **14** (1974) 431.
32. J. C. JOUBERT, T. SHIRK, W. B. WHITE and R. ROY, *Mater. Res. Bull.* **3** (1968) 671.
33. I. MANNING and G. P. MUELLER, *Comp. Phys. Commun.* **7** (1974) 85.
34. A. ALI, W. A. GRANT and P. J. GRUNDY, *Phil. Mag. B* **37**(3) (1978) 353.
35. R. O'NEILL, *Appl. Stat.* **20**(3) (1971) 338.

Received 11 April
and accepted 26 September 1985